Large-eddy simulation of a turbulent buoyant helium plume

By G. Blanquart AND H. Pitsch

1. Motivation and objectives

The numerical simulation of a turbulent buoyant plume remains challenging from a modeling point of view due to the presence of an inverse energy cascade. In the presence of gravity, a density stratification with heavy fluid on top of light fluid forms at the edges of the plume and is unstable subject to Rayleigh-Taylor instabilities. Slowly, velocity and density fluctuations appear at the very small scales. These fluctuations then rapidly grow in size and magnitude and eventually interact with the large-scale motion of the turbulent flow. The puffing cycles encountered in turbulent buoyant plumes is just one example of the very complex interaction between small and large scales features of the turbulent flow.

The purpose of this work is to perform a Large Eddy Simulation (LES) of a turbulent buoyant helium plume and to develop a new subgrid-scale model tailored for the simulation of buoyancy-driven flows. The article is organized as follows. The first section details the numerical methods and models used for the simulation. In the second section, the results using LES are presented and analyzed with a focus on the frequency response of the numerical simulation.

2. Numerical setup

The present work is performed with the NGA code (Desjardins *et al.* 2008). The NGA code is a 3-D finite difference structured code which solves for the low-Mach number Navier-Stokes equations using a fractional-step method (Kim & Moin 1985). The code relies on high accuracy variable density energy conserving finite difference schemes of arbitrary order. These schemes were found to be highly suited for the simulation of variable density turbulent flows and have already been used for the simulation of various configurations including a momentum-driven helium/air jet (Desjardins *et al.* 2008).

2.1. *Governing equations*

The NGA code solves for the filtered low-Mach number Navier-Stokes equations which consist of the filtered continuity equation

$$\frac{\partial \overline{\rho}}{\partial t} + \frac{\partial \left(\overline{\rho}\widetilde{u}_i\right)}{\partial x_i} = 0 \tag{2.1}$$

and the filtered momentum equation

$$\frac{\partial \overline{\rho}\widetilde{u}_j}{\partial t} + \frac{\partial \left(\overline{\rho}\widetilde{u}_j\widetilde{u}_i\right)}{\partial x_i} = -\frac{\partial \overline{p}}{\partial x_j} + \frac{\partial \overline{\tau}_{ij}}{\partial x_i} + \frac{\partial \overline{\tau}_{ij}^{SGS}}{\partial x_i} + \overline{\rho} g_i \,, \tag{2.2}$$

where g_i is the gravity vector. The viscous terms ($\overline{\tau}_{ij}$) and the Reynolds stress ($\overline{\tau}_{ij}^{SGS}$) terms are given by

$$\overline{\tau}_{ij} = \overline{\mu}\left(\frac{\partial \widetilde{u}_j}{\partial x_i} + \frac{\partial \widetilde{u}_i}{\partial x_j}\right) \tag{2.3}$$

and

$$\overline{\tau}_{ij}^{SGS} = \overline{\rho}\left(\widetilde{u}_i\widetilde{u}_j - \widetilde{u_i u_j}\right) . \tag{2.4}$$

In the present work, both the filtered density ($\overline{\rho}$) and the filtered dynamic viscosity ($\overline{\mu}$) are obtained through a mixing model and are expressed as a function of a conserved scalar Z which describes the gas mixture composition.

The filtered transport equation for the mixture fraction Z is written as

$$\frac{\partial \overline{\rho}\widetilde{Z}}{\partial t} + \frac{\partial}{\partial x_i}\left(\overline{\rho}\widetilde{u}_i\widetilde{Z}\right) = \frac{\partial \overline{g}_i}{\partial x_i} + \frac{\partial \overline{g}_i^{SGS}}{\partial x_i} \tag{2.5}$$

where the molecular diffusion term is given by

$$\overline{g}_i = \overline{\rho}\widetilde{D}\frac{\partial \widetilde{Z}}{\partial x_i} \tag{2.6}$$

and the turbulent scalar flux term is

$$\overline{g}_i^{SGS} = \overline{\rho}\left(\widetilde{u}_i\widetilde{Z} - \widetilde{u_i Z}\right) . \tag{2.7}$$

Similarly to the density and the viscosity, the filtered kinematic diffusivity ($\widetilde{D}$) is expressed as a function of the conserved scalar Z.

2.2. *Mixture properties*

At every point in the domain, the composition of the gas phase corresponds to a mixture between the helium and the air streams. The air stream is composed of molecular nitrogen (N_2, 79% by volume) and molecular oxygen (O_2, 21% by volume). The helium stream is composed mainly of helium (He, 96.4% by volume) and contains traces of molecular oxygen (O_2, 1.9% by volume) and acetone (CH_3COCH_3, 1.7% by volume). The temperature and pressure conditions are, respectively, $T = 283\,\mathrm{K}$ and $P = 0.799\,\mathrm{bar}$.

Following a similar approach as used for flamelet-based models, the diffusivity coefficient of all species is assumed to be the same. As a result, the mass fraction of the different species are simple linear functions of the mixture fraction Z, and the properties of the gas mixture are only function of the mixture fraction

$$\rho = \rho(Z)\,,\ \mu = \mu(Z)\,,\ D = D(Z)\,. \tag{2.8}$$

However, in the flamelet approach, the diffusivity coefficient is evaluated assuming unity Lewis number for all species. While this assumption is adequate for temperature diffusion dominated flows, the present configuration corresponds to constant temperature. In addition, the Lewis number of helium is very different from unity. Therefore, a different procedure is used. Observing that the binary diffusion coefficients of helium in nitrogen and in oxygen are almost the same, the diffusivity is evaluated as the binary diffusion coefficient of helium in air. The resulting kinematic diffusion coefficient does not depend upon mixture fraction

$$D \approx 8 \cdot 10^{-5}\,\mathrm{m}^2 \cdot \mathrm{s}^{-1} \tag{2.9}$$

In the LES framework, the Reynolds-filtered mixture properties are needed for the

simulation. The evaluation of the mean properties usually requires knowledge of the subgrid-scale probability density function (PDF) of the mixture fraction which is typically expressed as a function of the Favre mean ($\widetilde{Z}$) and variance ($\widetilde{Z''^2}$) of the mixture fraction. However, in the present case, the dynamic viscosity and kinematic diffusivity are only weak functions of the mixture fraction. In addition, since the mass fractions of the different species are linear functions of the mixture fraction, the Reynolds-filtered density is only a function of the Favre mean mixture fraction

$$\overline{\rho} = \overline{\rho}(\widetilde{Z}) \,, \overline{\mu} = \overline{\mu}(\widetilde{Z}) \,, \widetilde{D} = D \,. \tag{2.10}$$

These properties are evaluated using the FlameMaster code (Blanquart *et al.* 2009) and are tabulated as a function of the mean mixture fraction.

2.3. *Subgrid-scale model*

In the present work, both the Reynolds stress term and the turbulent scalar flux term are modeled using a dynamic Smagorinsky model. The subgrid-scale terms take the following form

$$\overline{\tau}_{ij}^{SGS} = \overline{\rho}\nu_t \left(\frac{\partial \widetilde{u}_j}{\partial x_i} + \frac{\partial \widetilde{u}_i}{\partial x_j} \right) \tag{2.11}$$

$$\overline{g}_i^{SGS} = \overline{\rho} D_t \frac{\partial \widetilde{Z}}{\partial x_i} \,, \tag{2.12}$$

where the eddy viscosity (ν_t) and eddy diffusivity (D_t) are expressed as

$$\nu_t = (C_S \Delta)^2 \, |\widetilde{S}| \tag{2.13}$$

$$D_t = (C_D \Delta)^2 \, |\widetilde{S}| \tag{2.14}$$

with Δ the size of the filter taken to be the volume equivalent cell size and $|\widetilde{S}|$ is the strain rate. In the present work, the Lagrangian model of Meneveau *et al.* (2000) was used to evaluate the Smagorinsky constants (C_S and C_D).

2.4. *Numerical setup*

Full details about the geometry of the configuration can be found in Tieszen *et al.* (1998), Blanchat (2001), and O'Hern *et al.* (2005). Therefore, only a brief description will be provided here. The overall geometry shown in Fig. 1 is axisymmetric with helium and air injected from two different locations. Helium is injected at the center of the domain through a 1 m diameter pipe surrounded by a 0.51 m wide flat plate. Air is injected through a 0.60 m wide annular pipe located 1.74 m below the helium source. Both inlets are modeled as uniform plug flows. The air inlet velocity is $v_{Air} = 0.139\,\mathrm{m \cdot s^{-1}}$, while the helium inlet velocity is $v_{He} = 0.299\,\mathrm{m \cdot s^{-1}}$. The helium velocity was lowered to account for the open area of the honeycomb (92%) (Blanchat 2001). The gravitational acceleration is taken to be $g = 9.81\,\mathrm{m \cdot s^{-2}}$.

The numerical simulation is performed on a cylindrical mesh with resolution $N_x \times N_r \times N_\theta = 192 \times 187 \times 64$. The time step size is constant $\Delta t = 6 \cdot 10^{-4}\,\mathrm{s}$ which corresponds to an averaged maximum convective CFL condition in x of $\sigma \approx 0.6$. The simulation is performed with the second-order accurate spatial scheme, and three sub-iterations are used for the fractional step time advancement. The mixture fraction is transported using the Bounded QUICK scheme (Herrmann *et al.* 2006) to assure that the mixture fraction remains bounded between 0 and 1.

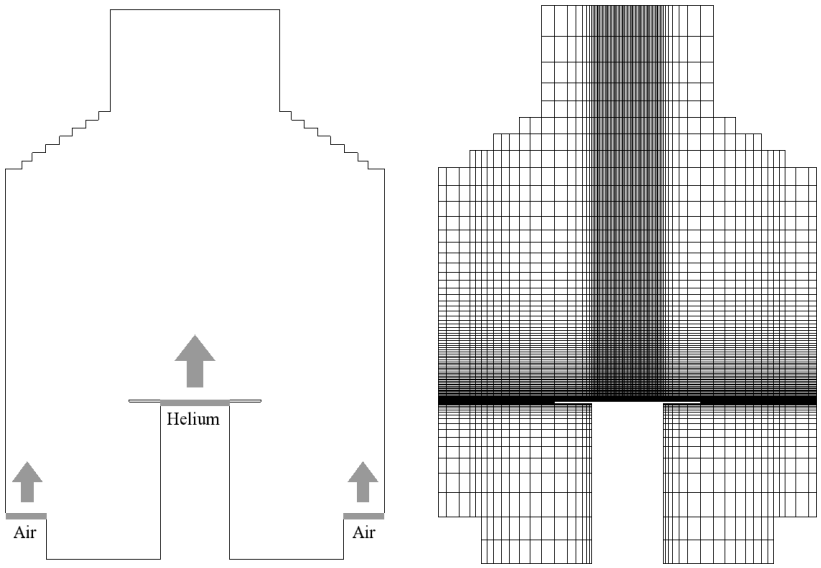

(a) Geometry (b) Mesh

FIGURE 1. Geometry and mesh of the configuration. For the mesh, only half the points are shown in x and a quater in y.

3. Results

3.1. *Puffing cycle*

The present turbulent buoyant helium plume is characterized by very distinct puffing dynamics. Rayleigh-Taylor instabilities start to form at the edge of the helium source and rapidly grow as they are convected inward and downstream. The resulting bubbles and spikes then interact with the large-scale features of the turbulent buoyant helium plume, ultimately leading to the formation of puffing cycles of various magnitudes. The puffing dynamics are easily observed by monitoring the temporal evolution of the vertical velocity inside the turbulent plume as plotted in Fig. 2. The time trace of the velocity is very similar to that reported by O'Hern *et al.* (2005). While the flow is fully turbulent and every puffing cycle is different, one can observe a distinct period for the oscillations. An analysis of the frequency of the time signal (recorded over about 30 cycles) shows a distinct peak located around 1.44 Hz. This value compares very favorably with the frequency of the puffing cycle measured experimentally (1.37 ± 0.1 Hz).

3.2. *Statistics*

Figure 3 shows a comparison of the Favre-averaged mean and root mean square axial velocity with experimental data. Two sets of experimental data are plotted as data points with positive and negative radii are available. The mean and rms axial velocity predicted by the current simulation compare very well with the experimental data, and the differences remain within the experimental uncertainties for all stations. The mean axial velocity increases downstream of the plume surface as a result of the acceleration by buoyancy forces. At the same time, the width of the plume decreases. Throughout the simulation, the magnitude of the velocity fluctuations remains quite large, about half that of the mean velocity. As shown in Fig. 2, the instantaneous velocity fluctuates

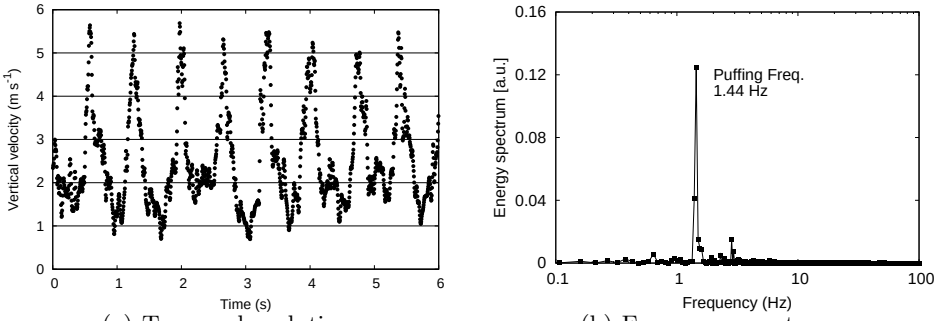

(a) Temporal evolution (b) Frequency spectrum

FIGURE 2. Temporal evolution and frequency spectrum of the vertical velocity on the centerline at 0.5 m above the helium source.

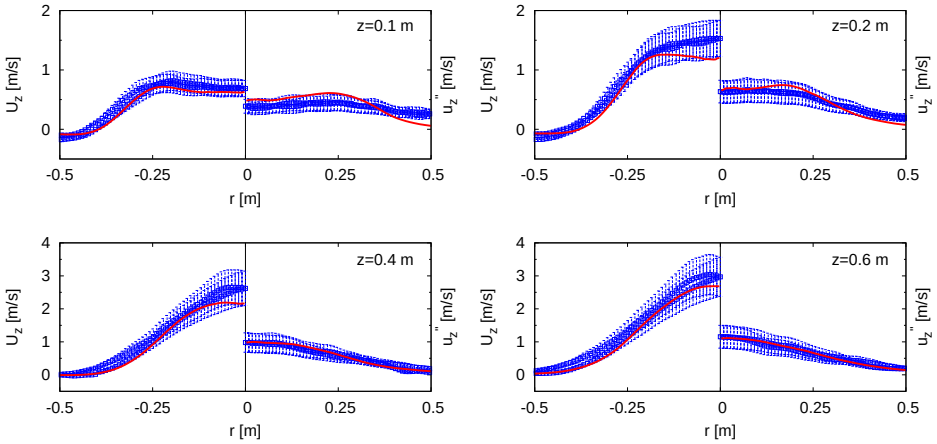

FIGURE 3. Radial profiles of Favre-averaged mean and rms of axial velocity at different axial positions above the helium source.

very strongly during a puffing cycle. As a result, in the present simulation, the rms velocities represents mainly the fluctuations of velocity between different time within one puffing cycle and do not adequately represent the turbulent fluctuations. In fact, the good agreement between the results of the numerical simulation and the experimental measurements is an evidence that the large-scale puffing cycle is accurately captured.

The comparison of the radial mean velocity and velocity fluctuations is also very good (Fig. 4). Because of acceleration of the helium by buoyancy forces, the plume entrains the surrounding air toward the centerline. This entrainment is stronger close to the plume surface and then decays downstream. Once again, the good agreement with the experimental data shows that the dynamics of the puffing cycles are correctly reproduced.

Figure 5 shows a comparison of the mean and rms helium mass fractions with experimental data. While the agreement with measurements is not as good as for the velocities, the comparison of the mean quantities remains favorable. However, the magnitude of the fluctuations in helium mass fraction appear to be over-estimated by the present numerical simulation. More precisely, the current simulation predicts a peak in the rms helium mass fraction corresponding to the location of the edge of the turbulent buoyant plume.

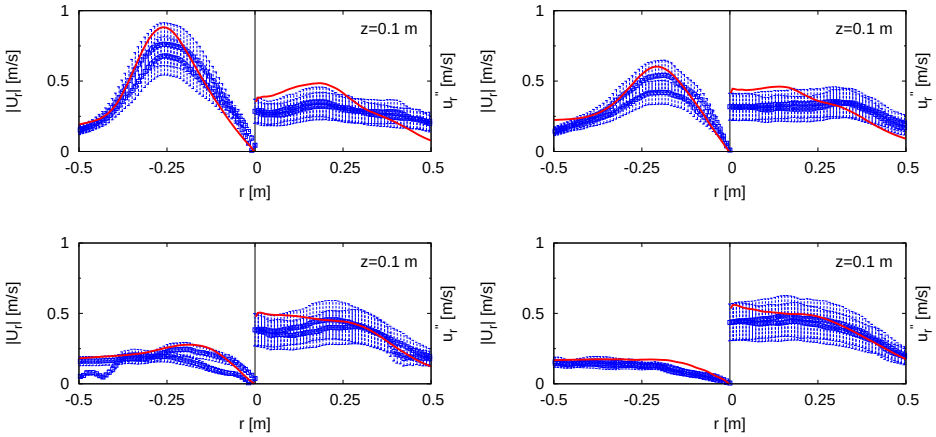

FIGURE 4. Radial profiles of Favre-averaged mean and rms of radial velocity at different axial positions above the helium source.

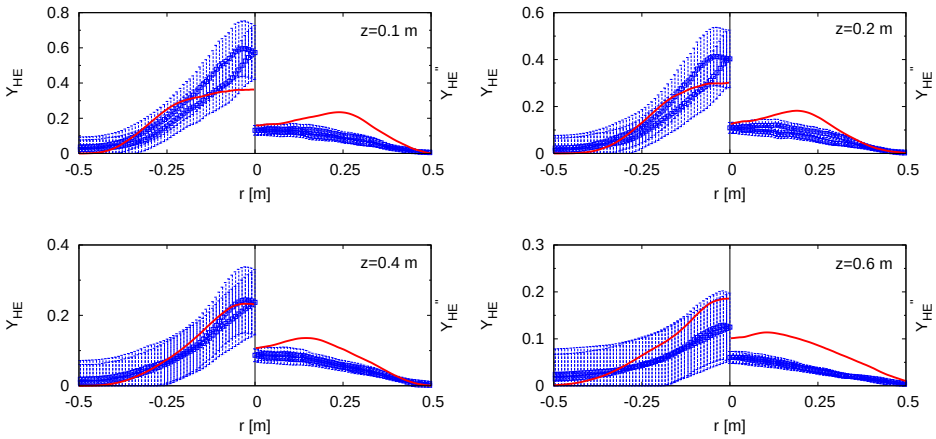

FIGURE 5. Radial profiles of Favre-averaged mean and rms of helium mass fraction at different axial positions above the helium source.

As observed previously for the axial velocity (Fig. 3), for higher distances above the plume surface, the edge of the plume gets closer to the centerline.

In order to better understand the differences between the simulation results and the experimental data, profiles of mean and rms quantities are plotted along the centerline (Fig. 6). As expected, both the mean velocity and the velocity fluctuations compare very well with the experimental measurements. On the other hand, the comparison of the helium mass fraction shows some differences. Very close to the plume surface (below 0.1 m), the numerical simulation predicts a strong decay of the mean mass fraction coupled with strong fluctuations in the helium concentration. These results are consistent with visual inspection of the flow showing a large intermittency of pure helium and pure air very close to the plume surface. While these different behavior might affect the evolution of the mean helium mass fraction downstream, its seem to have little effect on the mean and rms velocities.

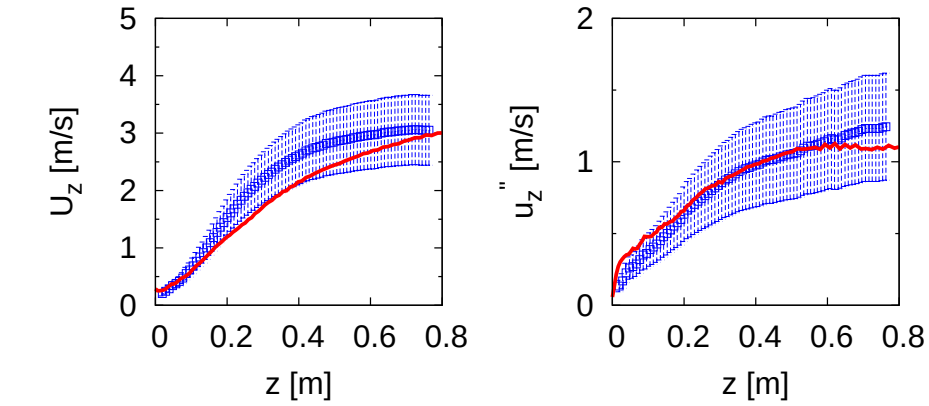

(a) Axial velocity

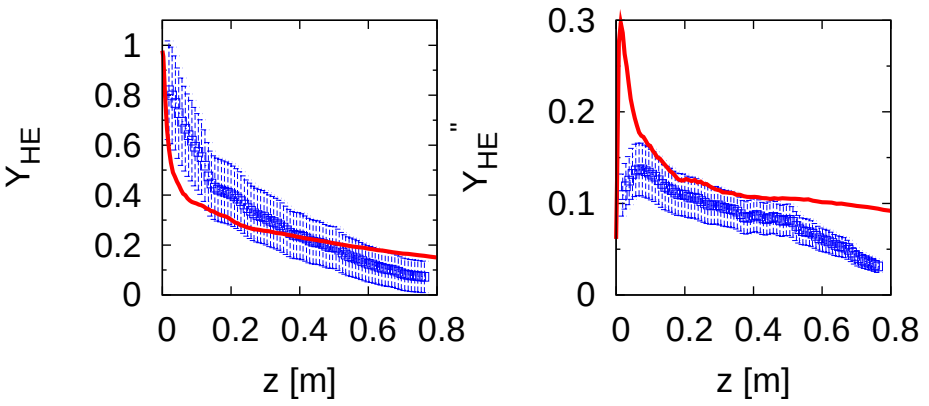

(b) Helium mass fraction

FIGURE 6. Axial profiles of Favre-averaged mean and rms.

4. Conclusion and future work

The complex dynamics of a turbulent buoyant helium plume have been investigated using Large Eddy Simulation. The properties of the gas mixture have been carefully estimated, for the growth of Rayleigh-Taylor instabilities is strongly controlled by density and scalar diffusion. The numerical results show that the present LES is able to capture accurately the large-scale puffing dynamics and its frequency. Futhermore, mean velocities and velocity fluctuations were found to compare favorably with experimental measurements.

Some discrepancies were found in various quantities very close to the helium source and further downstream. Very close to the helium source, the flow transitions rapidly from laminar to turbulent. While these differences do not appear to cause any effect on the flow downstream, a better treatment of the injection of helium through the honeycomb should be considered. Further downstream, the evolution of the mean helium concentration deviates from experimental measurements, and the concentration fluctuations are over-

estimated. These discrepancies highlight insufficient subgrid-scale mixing, characteristic of standard dynamic Smagorinsky models. A better subgrid-scale model tailored for buoyancy driven flows should be derived to properly account for subgrid-scale mixing due to the growth of Rayleigh-Taylor instabilities.

REFERENCES

Blanchat, T. K. 2001 Characterization of the air source and the plume source at FLAME. *Tech. Rep.* SAND2001-2227, Albuquerque, NM, Sandia National Laboratories.

Blanquart, G., Pepiot-Desjardins, P. & Pitsch, H. 2009 Assessing uncertainties in numerical simulations of simple reacting flows using the FlameMaster code. *Comb. Theory Model.*, in preparation.

Desjardins, O., Blanquart, G., Balarac, G. & Pitsch, H. 2008 High order conservative finite difference scheme for variable density low Mach number turbulent flows. *J. Comp. Phys.* **227** (15), 7125–7159.

Herrmann, M., Blanquart, G. & Raman, V. 2006 Flux corrected finite volume scheme for preserving scalar boundedness in reactive large-eddy simulations. *AIAA J.* **44** (12), 2879–2886.

Kim, J. & Moin, P. 1985 Application of a fractional-step method to incompressible Navier-Stokes equations. *J. Comp. Phys.* **59** (2), 308–323.

Meneveau, C., Lund, T. S. & Cabot, W. H. 2000 A Lagrangian dynamic subgrid-scale model of turbulence. *J. Fluid Mech.* **319**, 353–385.

O'Hern, T. J., Weckman, E. J., Gerhart, A. L., Tieszen, S. R. & Schefer, R. W. 2005 Experimental study of a turbulent buoyant helium plume. *J. Fluid Mech.* **544**, 143–171.

Tieszen, S. R., O'Hern, T. J., Schefer, R. W. & Perea, L. D. 1998 Spatial and temporal resolution of fluid flows: LDRD final report. *Tech. Rep.* SAND98-0338, Albuquerque, NM, Sandia National Laboratories.